

# Experimental determination of scattering matrices of randomly oriented fly ash and clay particles at 442 and 633 nm

O. Muñoz,<sup>1</sup> H. Volten, J. F. de Haan, W. Vassen, and J. W. Hovenier<sup>2</sup>

Department of Physics and Astronomy, Free University, Amsterdam, Netherlands

**Abstract.** We present measurements of the scattering angle distribution of the whole scattering matrix for randomly oriented particles of three mineral samples: fly ash, green clay, and red clay at 442 and 633 nm. Fly ash consists of aggregates of nearly spherical particles while green clay and red clay particles represent irregular compact particles. We compare the measured results for fly ash with an experimentally determined average scattering matrix which is based on measurements for a broad selection of irregular mineral aerosol particles. We find that the scattering matrix of our polydisperse sample of aggregates of nearly spherical particles differs considerably from that of compact particles. In addition, the angular distribution of the elements of the scattering matrix (except  $F_{22}(\theta)/F_{11}(\theta)$ ) for fly ash particles seem to be dominated by the single monomers. The effects of small differences in composition on the scattering behavior have also been studied by comparing our experimental results for green clay particles with those obtained by *Volten et al.* [2001] for red clay particles at the same wavelengths.

## 1. Introduction

Most solid particles in terrestrial and planetary atmospheres, and other solar system bodies such as asteroids and comets, consist of irregular mineral particles. These mineral particles seem to occur in a broad range of shapes [e.g., *Okada et al.*, 1987; *Warren et al.*, 1997] and to be distributed in size [e.g., *d'Almeida et al.*, 1991]. In many cases, scattered light is the only tool we have to retrieve information about the structure and origin of these celestial bodies and their atmospheres. Therefore it is important to study the scattering of light by randomly oriented polydisperse irregular particles with sizes comparable to the wavelength of the incident light.

*Lumme* [2000] suggested that in a fairly broad sense, small irregular particles can be divided in two classes: aggregated and compact particles. Aggregated particles seem to be ubiquitous in space: molecular clouds, interplanetary and cometary dust, and planetary aerosols [e.g., *Greenberg and Gustafson*, 1981; *West and Smith*, 1991; *Wurm and Blum*, 1998]. Compact mineral particles have been found in the Earth's atmosphere [*Prospero et al.*, 1981; *Rietmeijer*, 1993], the atmosphere of Mars [*Moroz et al.*, 1994], comets [*Jäger et al.*, 1994; *Colangeli et al.*, 1995], meteorites [*Weiss-Wrana*, 1983],

and circumstellar and interstellar matter [*Molster et al.*, 1999].

Regarding light scattering by small particles, there are no accurate numerical codes that can handle the irregularity and broad size range of the compact particles we find in nature (see *Mishchenko et al.* [2000a] for a detailed description of the advantages and constraints of the more frequently used numerical codes for nonspherical particles). Aggregated particles have been also under theoretical study by many authors [e.g., *West*, 1991; *Mishchenko et al.*, 1995; *Mackowski*, 1995; *Mackowski and Mishchenko*, 1996; *Lumme et al.*, 1997; *Xing and Hanner*, 1997; *Haudebourg et al.*, 1999; *Yanamandra-Fisher and Hanner*, 1999; *Xu and Gustafson*, 1999]. However, even the faster methods cannot give accurate results for natural polydisperse samples of aggregated particles.

Therefore the experimental study of the scattering behavior of polydisperse aggregates and compact irregular particles is of main importance. However, results of only a small number of laboratory measurements are available in the literature.

The microwave analog technique has been used to study light-scattering properties of particles for many years [see *Gustafson*, 2000, and references therein]. With this technique the light-scattering problem is scaled to longer wavelengths and to larger particle sizes allowing accurate sample characterization. A disadvantage of such measurements is that they cannot be performed for natural polydisperse samples within a reasonable time.

Copyright 2001 by the American Geophysical Union.

Paper number 2000JD000164.  
0148-0227/01/2000JD000164\$09.00

Measurements at visible wavelengths using laser light scattered by an ensemble of particles have been reported by different authors. This method has been used to measure the angular distribution of all elements of the scattering matrix [e.g., *Perry et al.*, 1978; *Holland and Gagne*, 1970; *Kwik et al.*, 1991; *Muñoz et al.*, 2000; *Volten et al.*, 2001] or just the phase function and the degree of linear polarization for unpolarized incident light as a function of the scattering angle [e.g., *Jaggard et al.*, 1981, *West et al.*, 1997]. *Böttiger et al.* [1980] published the results of such an experimental study of the scattering matrix as a function of the scattering angle for randomly oriented monodisperse aggregates of nearly identical micron-sized latex spheres. Their measurements for bispheres have been quantitatively reproduced using the superposition T-matrix method as described by *Mishchenko and Mackowski* [1996].

In this work we present unique measurements at two wavelengths, 442 and 633 nm, of the (relative) scattering angle distribution of the complete scattering matrix of three samples of polydisperse randomly oriented particles as examples of the two classes of small irregular particles: fly ash (aggregates) and green clay and red clay (compact particles). There are theoretical indications that aggregates of spherical particles show scattering properties that differ substantially from those of compact mineral particles with similar refractive indices and sizes [*Mishchenko et al.*, 1995; *Mackowski and Mishchenko*, 1996]. The main purpose of this paper is to report an experiment that shows how scattering properties of polydisperse aggregates may differ from those of compact irregular mineral particles with similar size distributions and refractive indices. For this purpose the measured results for fly ash particles have been compared to the measured results for green clay and red clay particles and the experimentally determined average scattering matrix for irregular mineral aerosol particles obtained by *Volten et al.* [2001]. This matrix (henceforth called the average scattering matrix) was obtained by measuring at two wavelengths (442 and 633 nm) the scattering matrices as functions of the scattering angle of seven different mineral samples (including red clay), all of which belong to the compact particles group but each having a different projected surface distribution and refractive index. The only property of fly ash that has no overlap with the properties of these samples is the shape of the particles.

The study of the scattering properties of fly ash particles is also important for another reason. Fly ash is a by-product (consisting mainly of clays) of the combustion of coal in electricity power plants. The strong influence on climate of anthropogenic atmospheric aerosols [see, e.g., *Charlson et al.*, 1992] is very well known. Therefore studying the scattering behavior of fly ash particles is useful in order to estimate their effect on climate in industrial regions where the concentration of this kind of anthropogenic aerosols can be high.

In experimental light scattering studies it is important to obtain well-characterized samples to be used in controlled laboratory measurements. For example, if we can obtain two samples for which just one of the physical parameters of the particles differs, we can isolate the effect of that parameter on the scattering behavior. This is not an easy matter because of the difficulty of finding the right samples for such measurements. However, our green clay and red clay samples fulfill this requirement very well. They contain particles having size distributions and shapes that are almost identical to each other but presenting small differences in composition. Thus we have studied the influence on the scattering behavior of differences in composition, since the influence of the other parameters (size distribution and shape) may be assumed to be negligible.

In summary, in section 2 we present a brief review of the theory involved in the experiments and a description of the experimental setup used to measure the entire scattering matrix at 442 and 633 nm. In section 3 the physical characteristics of our samples are presented. Results of our experiments are shown in section 4.1. In section 4.2 we compare the results obtained for fly ash particles with the experimentally determined average aerosol scattering matrix [*Volten et al.*, 2001]. In addition, the measured results have been compared to computational results. The comparison is done in a qualitative way, since we have not found published computational results for a sufficiently broad size distribution or large enough size parameters of the constituent particles. In section 4.3 we compare the measured scattering matrices as functions of the scattering angle for green clay particles with those obtained by *Volten et al.* [2001] for red clay particles and the average aerosol scattering matrix. Conclusions are presented in section 5.

## 2. Some Concepts of Light Scattering and the Experimental Setup

The flux and polarization of a quasi-monochromatic beam of light can be represented by a column vector  $\mathbf{I} = \{I, Q, U, V\}$ , also called Stokes vector [*Van de Hulst*, 1957; *Hovenier and van der Mee*, 1983]. Here  $I$  is proportional to the total flux of the beam. The Stokes parameters  $Q$  and  $U$  represent differences between two components of the flux for which the electric field vectors oscillate in mutual orthogonal directions. The Stokes parameter  $V$  is the difference between two oppositely circularly polarized components of the flux. A plane through the direction of propagation of the beam is chosen as a plane of reference for the Stokes parameters.

If light is scattered by an ensemble of randomly oriented particles and time reciprocity applies, as is the case in our experiment, the Stokes vectors of the incident beam and the scattered beam are related by a  $4 \times 4$

scattering matrix, for each scattering angle, as follows [Van de Hulst, 1957, section 5.22],

$$\begin{pmatrix} I_{sc} \\ Q_{sc} \\ U_{sc} \\ V_{sc} \end{pmatrix} = \frac{\lambda^2}{4\pi^2 D^2} \begin{pmatrix} F_{11} & F_{12} & F_{13} & F_{14} \\ F_{12} & F_{22} & F_{23} & F_{24} \\ -F_{13} & -F_{23} & F_{33} & F_{34} \\ F_{14} & F_{24} & -F_{34} & F_{44} \end{pmatrix} \begin{pmatrix} I_{in} \\ Q_{in} \\ U_{in} \\ V_{in} \end{pmatrix}, \quad (1)$$

where the subscripts  $i$  and  $s$  refer to the incident and scattered beam, respectively,  $\lambda$  is the wavelength of the incident beam, and  $D$  is the distance from the ensemble to the detector. The matrix with elements  $F_{ij}$  is called the scattering matrix. Its elements depend on the scattering angle  $\theta$  but not on the azimuthal angle. Here the plane of reference is the scattering plane, that is, the plane containing the beams of incident and scattered light. The elements  $F_{ij}$  contain information about the size distribution, shape, and refractive index of the scatterers. It follows from (1) that there are 10 matrix elements to be determined. This number is further reduced when a scattering sample consists of randomly oriented particles with equal amounts of particles and their mirror particles. In that case, the four elements  $F_{13}(\theta)$ ,  $F_{14}(\theta)$ ,  $F_{23}(\theta)$ , and  $F_{24}(\theta)$  are zero over the entire angle range [Van de Hulst, 1957].

A detailed description of the experimental setup that we used to measure the scattering matrix is given by Hovenier [2000]. A brief summary is given here. We use either a HeNe laser (633 nm, 5 mW) or a HeCd laser (442 nm, 40 mW) as a light source. The laser light passes through a polarizer oriented at an angle  $\gamma_P$  and an electro-optic modulator oriented at an angle  $\gamma_M$  (angles of optical elements refer to the angle between their optical axis and the scattering plane, measured counterclockwise when looking in the direction of propagating of the light). The modulated light is subsequently scattered by the ensemble of randomly oriented particles located in a jet stream produced by an aerosol generator. The scattered light passes through a quarter-wave plate oriented at an angle  $\gamma_Q$  and an analyzer oriented at an angle  $\gamma_A$  (both optional) and is detected by a photomultiplier tube which moves in steps along a ring. A range in scattering angles is covered from approximately  $5^\circ$  (nearly forward scattering) to about  $173^\circ$  (nearly backward scattering). A monitor, that is, a photomultiplier placed at a fixed position, is used for normalization purposes. We employ polarization modulation in combination with lock-in detection to determine all elements of the  $4 \times 4$  scattering matrix, in the sense that we obtain the phase (scattering) function,  $F_{11}(\theta)$ , in a relative way and the other elements divided by  $F_{11}(\theta)$ . The procedure during the measurements is as follows: the aerosol jet in the scattering center is produced by an aerosol generator, which consists of a reservoir, a brush, and an airflow control. The reservoir is filled with the aerosol sample which is pushed upwards against a rotating brush. An airflow blows the particles from the brush through a tube in the scattering zone, where the

light from the laser beam is scattered by the aerosols. In order to investigate whether the shape of the particles had changed after passing the aerosol generator, we put a glass plate under the aerosol jet to recover the sample as it was measured during the experiment. We look at it through a microscope and compare the particles with particles of the same sample that are not used for the experiment. In all cases the particles before and after the experiment did not look different.

Errors in the measured matrix elements originate from fluctuations in the measured signal or signals. For each data point at a given scattering angle, 720 measurements are conducted in about 2 s. The values obtained for the measured matrix elements or combinations of matrix elements are the average of several data points (about five or more) and the corresponding experimental error is the standard deviation in these (see also Volten *et al.* [2001]).

We investigated the reliability of the measurements presented in this paper by applying the Cloude coherency test [Hovenier and van der Mee, 1996]. We found that for all matrix elements the values measured for scattering angles from  $5^\circ$  to  $173^\circ$  are in agreement with the Cloude coherency test within the experimental errors.

Measurements with water droplets were done in order to test the setup. Since the water droplets had spherical shapes, we could compare the experimental results with those obtained from Mie calculations. We found excellent agreement over the entire angle range measured for all scattering matrix elements. The results of the experiments and calculations for water droplets have been published by Volten *et al.* [2001].

### 3. Characterization of the Samples

In this section we discuss physical characteristics of the samples considered in this paper. They consist of small particles of fly ash, green clay, and red clay. In particular, we consider the shapes, chemical compositions, the size distributions and the complex refractive indices of the particles.

#### 3.1. Origin and Shapes

Fly ash can be produced by a number of processes, such as the combustion of coal in power stations, the gasification of coal and the combustion of waste, each of which may lead to fly ashes with specific characteristics. Our sample of fly ash originates from the inorganic fraction, mainly clays, of the combustion of powdered coal in an electricity power plant. It consists of aggregates of nearly spherical particles. A scanning electron microscope (SEM) photograph of the fly ash particles is presented in Figure 1 (top). Our clay particles are natural particles that, in contrast, exhibit irregular shapes with a layered structure. In Figure 1 (bottom) we present a SEM picture of green clay. Red clay particles also present the typical layered structure

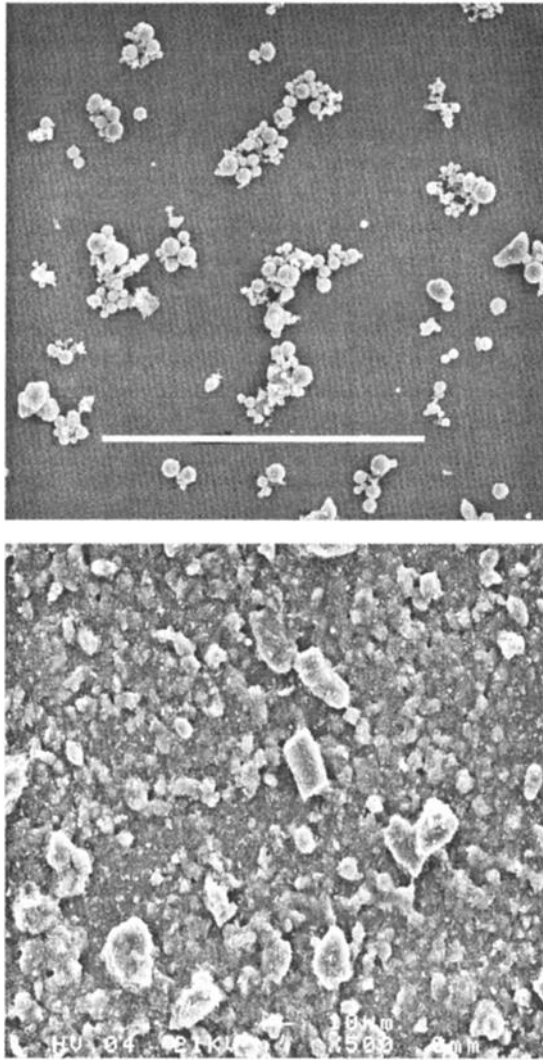


**Figure 1.** Scanning electron microscope (SEM) photographs of the (top) fly ash particles and (bottom) green clay particles. The white bar denotes (top) 100  $\mu\text{m}$  and (bottom) 10  $\mu\text{m}$ .

of clay particles. See *Volten et al.* [2001] for a SEM picture of red clay particles.

### 3.2. Particle Sizes

The projected surface area distributions have been measured by using a Fritsch laser particle sizer [*Konert and Vandenberghe, 1997*]. Figure 2 (top) shows normalized projected surface area distributions  $S(\log r)$  as functions of  $r$  in micrometers on a logarithmic scale for fly ash, green clay, and red clay particles. Here  $r$  is the radius of a sphere having the same projected surface area as the irregular particle has, and  $S(\log r)d \log r$  gives the relative contribution by spheres with radii in the size range  $[\log r, \log r + d \log r]$  to the total projected surface per unit volume of space. This implies that equal areas under a curve correspond to equal contributions to the total projected surface. Since for irregular particles larger than about 1  $\mu\text{m}$ , the projected surface

area is proportional to the scattering cross section [*Hodkinson, 1963*], Figure 2 gives us information about how particles of different size contribute to the scattering.

In Figure 2 (bottom), normalized number distributions,  $N(\log r)$  are presented, since these are often used in calculations and reported in the literature. Here  $N(\log r)d \log r$  gives the relative contribution by spheres with radii in the size range  $[\log r, \log r + d \log r]$  to the total number of spheres per unit volume of space.  $N(\log r)$  was computed from the corresponding  $S(\log r)$ . The normalized number distributions of the samples studied in this work are similar to number distributions of mineral samples found in the Earth's atmosphere [*d'Almeida et al., 1991*]. Although the SEM pictures are not necessarily representative for the size distributions of the aggregates as a whole (for that purpose we refer Figure 2), we can make an estimate of the size of the constituent particles in the aggregates of the fly ash sample. It appears that most of the constituent spheres

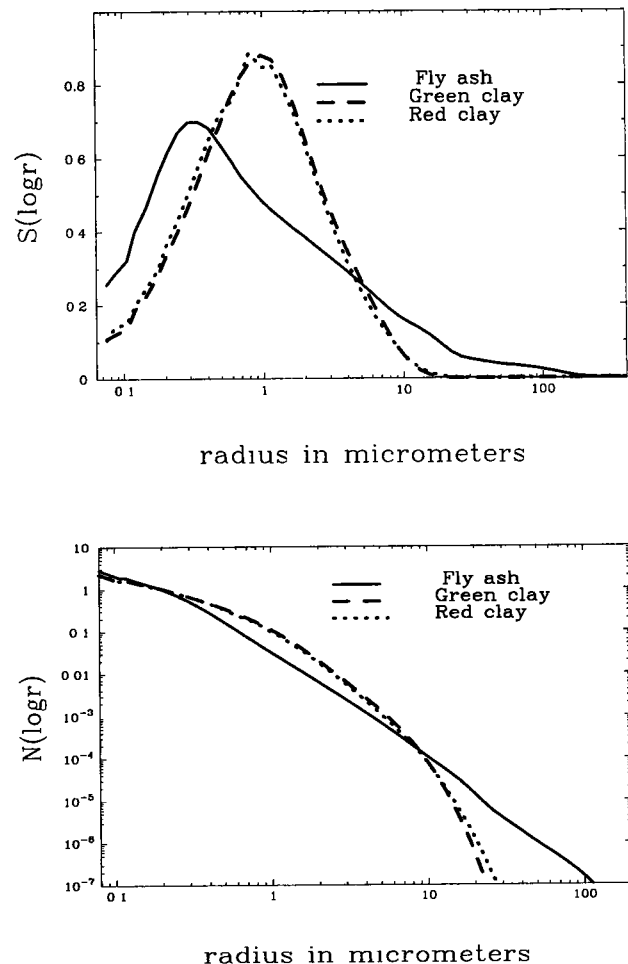


**Figure 2.** (top) Measured projected normalized surface area distributions, and (bottom) corresponding normalized number distributions, of the fly ash, green clay, and red clay particles. The distributions are plotted as functions of the radius in micrometers on a logarithmic scale.

**Table 1.** Overview of Properties of the Aerosol Samples Studied

Sample	$r_{\text{eff}}$ , $\mu\text{m}$	$v_{\text{eff}}$	Color
Fly ash	3.65	10.9	grey
Green clay	1.55	1.4	green
Red clay	1.50	1.6	red

in the fly ash aggregates have diameters  $d$  such that their size parameters ( $x = \pi d/\lambda$ ) are larger than 15 at 442 nm and larger than 10 at 633 nm.

Values of the effective radius ( $r_{\text{eff}}$ ) and variance ( $v_{\text{eff}}$ ) of each sample are given in Table 1. These two parameters are defined as follows:

$$r_{\text{eff}} = \frac{\int_0^\infty r \pi r^2 n(r) dr}{\int_0^\infty \pi r^2 n(r) dr}, \quad (2)$$

$$v_{\text{eff}} = \frac{\int_0^\infty (r - r_{\text{eff}})^2 \pi r^2 n(r) dr}{r_{\text{eff}}^2 \int_0^\infty \pi r^2 n(r) dr}, \quad (3)$$

where  $n(r)dr$  is the fraction of the total number of spheres with radii in the size range  $[r, r+dr]$  per unit volume of space [Hansen and Travis, 1974]. Here  $n(r)$  is computed from  $N(\log r)$ .

### 3.3. Refractive Indices and Composition

In Table 2 we present the most abundant minerals of the samples considered in this paper. The exact values of the refractive indices of the samples are unknown. Based on literature values [Kerr, 1959; Tröger et al., 1971; Egan and Hilgeman, 1979; Gerber and Hindman, 1982; Klein and Hurlbut, 1993], we can safely assume that at visual wavelengths the real part of the refractive index lies between 1.5 and 1.7, while the imaginary parts likely lie in the range between  $10^{-2}$  and  $10^{-5}$ . Since the three samples have similar compositions, we estimate their refractive indices to be also very similar except, perhaps, for the imaginary part of the colored clay particles.

## 4. Results and Discussion

### 4.1. Measurements

In Figures 3-5 we present elements of the complete scattering matrices at 442 and 633 nm as functions of the scattering angle for the randomly oriented particles of fly ash, green clay, and red clay. For convenience, we normalized all matrix elements (except  $F_{11}$  itself) to  $F_{11}$ , that is, we consider  $F_{ij}/F_{11}$ , with  $i, j = 1$  to 4. All scattering functions or phase functions  $F_{11}(\theta)$  considered in this paper are shown on a logarithmic scale and are normalized to 1 at  $30^\circ$ .

Instead of  $F_{12}/F_{11}$  we have plotted

$$-F_{12}/F_{11} = \frac{I_r - I_l}{I_r + I_l}, \quad (4)$$

where, for unpolarized incident light,  $I_r$  and  $I_l$  represent the flux of the scattered light polarized perpendicular and parallel to the plane of scattering, respectively.

We refrained from showing the element ratios  $F_{13}(\theta)/F_{11}(\theta)$ ,  $F_{14}(\theta)/F_{11}(\theta)$ ,  $F_{23}(\theta)/F_{11}(\theta)$ , and  $F_{24}(\theta)/F_{11}(\theta)$  since they were found to be zero over the entire range of scattering angles within the accuracy of the measurements. This is in agreement with the assumption of randomly oriented particles with equal amounts of particles and their mirror particles [Van de Hulst, 1957]. Therefore in this case  $-F_{12}/F_{11}$  equals the degree of linear polarization of the scattered light for incident unpolarized light. The experimental errors are indicated in Figures 3-5 by error bars. When no error bar is shown, the value of the standard deviation is smaller than the symbol plotted.

The results are presented together with the average scattering matrix obtained by Volten et al. [2001]. This average was obtained from seven samples of irregularly shaped mineral particles including red clay particles at two wavelengths (442 and 633 nm). The main interest of this average is that, although the seven samples of irregularly shaped mineral particles present a broad range in refractive indices and size distributions, the experimentally determined values of the scattering matrix elements, when plotted as functions of the scattering angle, are confined to rather limited domains. Physical characteristics (refractive indices and size distributions) of the samples of fly ash and green clay considered in this paper lie within the values presented by the samples studied by these authors, but fly ash particles differ considerably in shape (see section 2.1).

### 4.2. Discussion of the Scattering Matrices of Fly Ash Particles

In Figure 3 we present the experimentally determined scattering matrices at 442 and 633 nm for the aggregates of nearly spherical fly ash particles, together with the average scattering matrix. Manifestations of non-sphericity are clearly present, for example, the ratios  $F_{33}(\theta)/F_{11}(\theta)$  and  $F_{44}(\theta)/F_{11}(\theta)$  differ from each other and the ratio  $F_{22}(\theta)/F_{11}(\theta)$  deviates considerably from

**Table 2.** Main Components of the Samples of Fly Ash, Green Clay, and Red Clay<sup>a</sup>

	Fly Ash	Green Clay	Red Clay
SiO <sub>2</sub>	48.0	50.6	50.2
Al <sub>2</sub> O <sub>3</sub>	25.4	14.1	20.0
Fe <sub>2</sub> O <sub>3</sub>	6.8	4.8	7.0
CaO	7.1	9.2	6.2
MgO	3.9	2.3	2.4
K <sub>2</sub> O	-	4.0	3.7
Mn	-	-	0.1
Na <sub>2</sub> O	1.2	0.2	-
P <sub>2</sub> O <sub>5</sub>	-	0.1	-
SO <sub>3</sub>	1.3	-	-
TiO <sub>2</sub>	0.2	-	-

<sup>a</sup>Units in percent by weight.

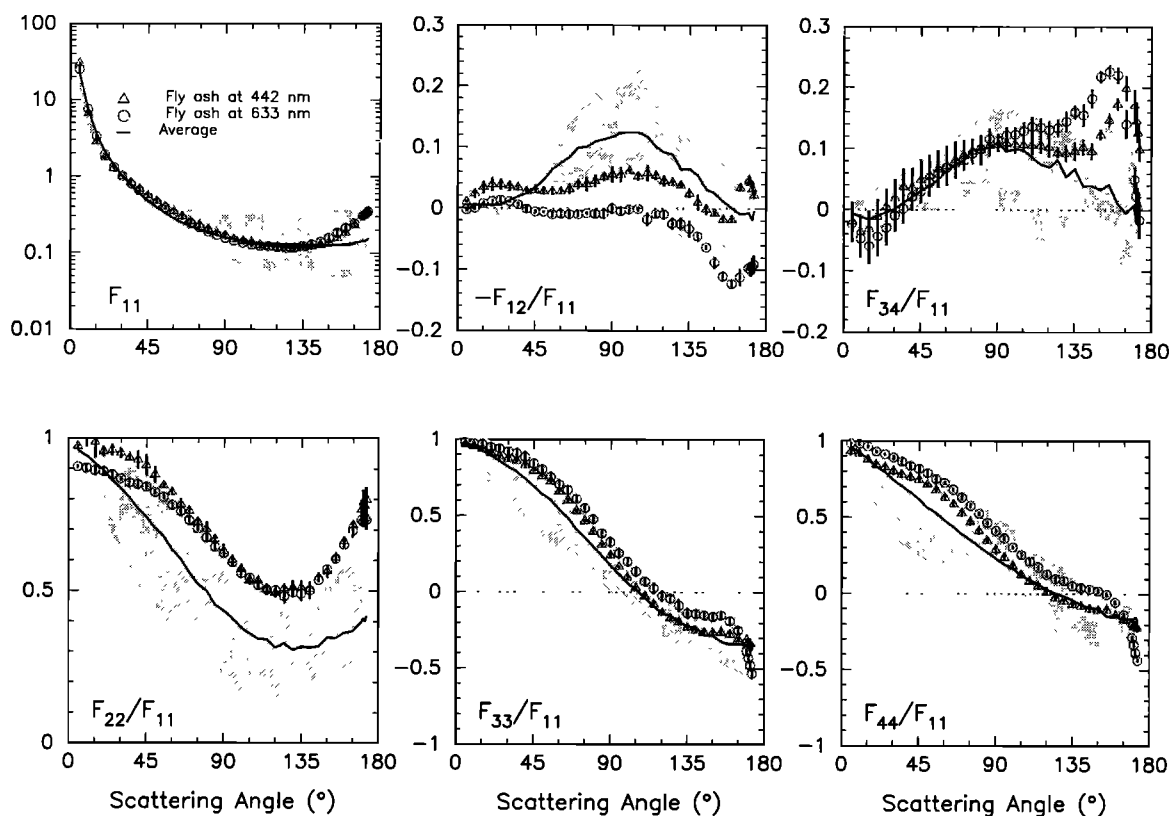


**Figure 3.** Measured scattering matrix as functions of the scattering angle for fly ash particles at 442 nm (triangles) and 633 nm (circles). The measurements are presented together with their error bars. In case no error bars are shown, they are smaller than the symbols. Solid lines correspond to the average mineral scattering matrix for compact particles. The domains occupied by the aerosol measurements presented by *Volten et al.* [2001] are indicated by shading.

unity. The measured scattering matrices of fly ash particles also do not follow the general trends presented by irregularly shaped compact particles [*Mishchenko et al.*, 2000b; *Volten et al.*, 2001] as will be discussed below.

For instance, the scattering functions  $F_{11}(\theta)$  for the fly ash particles show a relatively strong increase at backscattering angles compared to experimental results obtained for green clay and red clay particles and the average scattering curve for irregular mineral particles. In Table 3 we present values of  $F_{11}(\theta)$  at  $173^\circ$ , divided by the measured minimum values over the scattering angle range from  $5^\circ$  to  $173^\circ$ ,  $(F_{11}(173^\circ)/F_{11\min})$ . We find a value of  $F_{11}(173^\circ)/F_{11\min}$  of 3.0 at both wavelengths for fly ash particles. This increase of  $F_{11}(\theta)$  at backscattering angles is reminiscent of results of Mie calculations for polydisperse spheres with similar size distributions as the constituent monomers of the aggregates. In contrast, for green clay and red clay particles and the average scattering matrix the values of  $(F_{11}(173^\circ)/F_{11\min})$  are close to 1 (1.1–1.2). These flat phase functions at large scattering angles seem to be commonly found for irregularly shaped particles [e.g., *Holland and Gagne*, 1970; *Perry et al.*, 1978; *Kuik et al.*, 1991; *West et al.*, 1997; *Muñoz et al.*, 2000; *Volten et al.*, 2001]. In contrast,  $F_{11}(\theta)$  curves for rounded particles [*Perry et al.*, 1978], randomly oriented packed clusters of spheres

[*Mackowski and Mishchenko*, 1996] and polydisperse randomly oriented bispheres [*Mishchenko et al.*, 1995] present an enhanced backward peak compared to irregularly shaped compact particles. Therefore the enhancement of  $F_{11}(\theta)$  at backscattering angles for the fly ash sample seems to be related to the shape of its particles, which are aggregates of spheres.

In Table 3 we also present the steepness of  $F_{11}(\theta)$  curves, defined as the measured maximum value of  $F_{11}(\theta)$  divided by the measured minimum value over the scattering angle range from  $5^\circ$  to  $173^\circ$ . The steepness of  $F_{11}(\theta)$  depends strongly on the effective size parameter of the particles, since forward diffraction peaks are steeper for large particles than for small particles. However, our measurements do not include the forward diffraction peaks for angles smaller than  $5^\circ$  and, in fact, we see that the green and red clay particles show larger steepnesses than the larger fly ash particles.

The measured  $-F_{12}(\theta)/F_{11}(\theta)$  curves for fly ash particles are found to differ appreciably from the average aerosol curve. In Tables 4 and 5 we present the main features of this function at 442 and 633 nm, respectively. The measured results for  $-F_{12}(\theta)/F_{11}(\theta)$  at 442 nm show positive values at almost all scattering angles with three relative maxima near  $25^\circ$ ,  $100^\circ$ , and  $170^\circ$ . The shape of the function at 633 nm is similar to that at 442

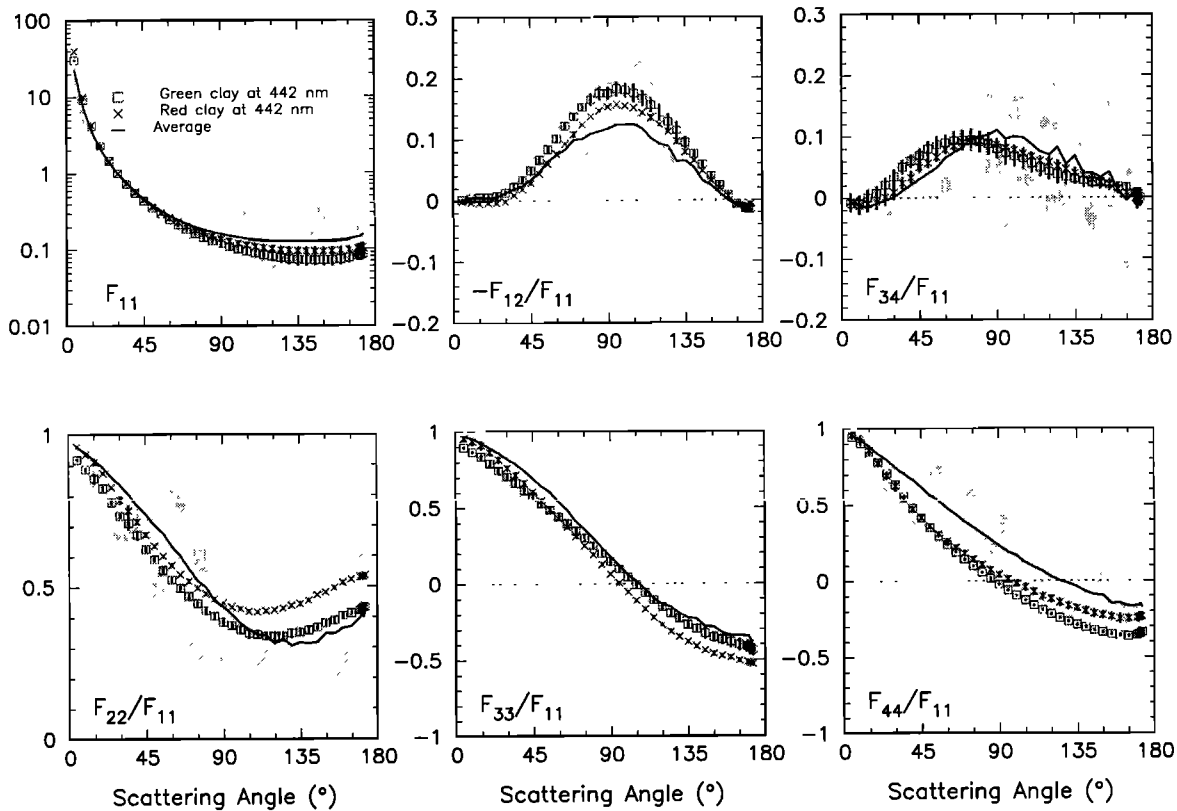


**Figure 4.** Comparison of the measured scattering matrix elements as a function of the scattering angle for green clay (squares) and red clay particles (crosses) at 442 nm. The measurements are presented together with their error bars. In case no error bars are shown, they are smaller than the symbols. Solid lines correspond to the average mineral scattering matrix. The domains occupied by the aerosol measurements presented by *Volten et al.* [2001] are indicated by shading.

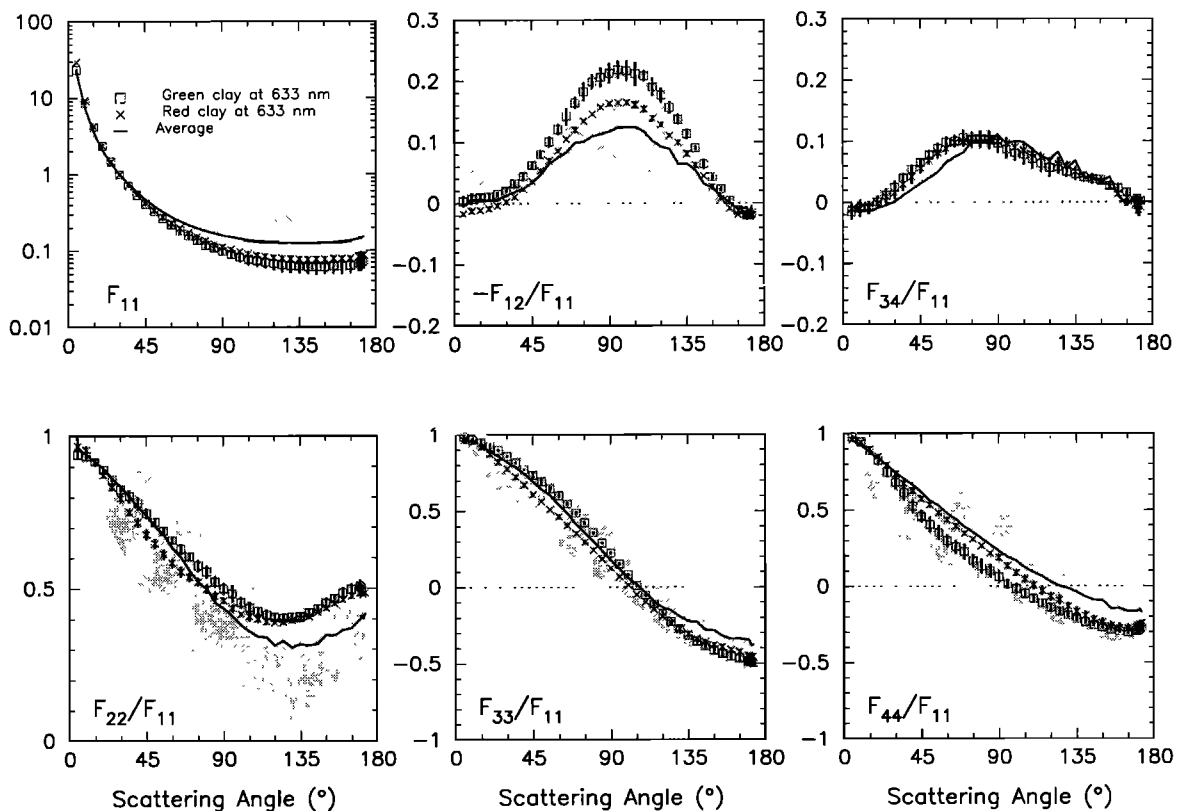


**Figure 5.** Same as Figure 4, but at 633 nm.

**Table 3.** Values of  $F_{11}(\theta)$  at  $173^\circ$  Divided by the Minimum Values Measured Over the Scattering Angle Range From  $5^\circ$  to  $173^\circ$  and Steepnesses of  $F_{11}(\theta)$  at 442 and 633 nm<sup>a</sup>

Sample	$F_{11}(173^\circ)/F_{11\min}$		Steepness	
	442 nm	633 nm	442 nm	633 nm
Fly ash	3.0	3.0	262	215
Green clay	1.1	1.1	423	392
Red clay	1.2	1.2	430	390
Av.Sc.M.	1.2		187	

<sup>a</sup>The results are compared with those obtained for the average mineral aerosol scattering matrix (Av.Sc.M.).

nm, but the values are nearly zero at side-scattering angles and become negative at backward directions with a minimum near  $160^\circ$  (see Table 5). Besides the differences in shape for  $-F_{12}(\theta)/F_{11}(\theta)$  relative to the average scattering curve, the values of the degree of linear polarization for the fly ash are generally lower. Low values of the degree of linear polarization were also found by *Bottiger et al.* [1980], for measurements on monodisperse quadruplets of micron sized spheres at 441.6 nm. According to *Gustafson and Kolokolova* [1999], the shape of  $-F_{12}(\theta)/F_{11}(\theta)$  and the amount of polarization depend strongly on the size parameter of the constituent particles of the aggregate. They find an oscillation around small polarization values when the size parameters of the constituent particles are of the order of 20 which is similar to the values of our particle constituents (see section 3.2).

The measured  $F_{34}(\theta)/F_{11}(\theta)$  for fly ash particles also presents appreciable deviations from the average scattering curve for compact irregular particles. This ratio presents a negative branch at small scattering angles and has a maximum at much higher angles ( $165^\circ$  and  $155^\circ$  at 442 and 633 nm, respectively see Tables 4 and 5). The shapes of  $-F_{12}(\theta)/F_{11}(\theta)$  and  $F_{34}(\theta)/F_{11}(\theta)$  resemble the result for polydisperse spheres with similar size distributions and refractive indices as the constituent particles of the aggregates [see e.g., *Perry et al.*, 1978; *Mishchenko et al.*, 1995].

Differences between the ratios  $F_{33}(\theta)/F_{11}(\theta)$  and  $F_{44}(\theta)/F_{11}(\theta)$  for fly ash particles compared to irregular mineral particles are largest at backscattering angles, especially at 633 nm. For the fly ash both  $F_{33}(\theta)/F_{11}(\theta)$  and  $F_{44}(\theta)/F_{11}(\theta)$  decrease suddenly at backscattering angles at 633 nm. This sudden decrease was also found

by *Mishchenko et al.* [1995] for spheres and polydisperse randomly oriented bispheres but was not found for irregular mineral particles such as the green and red clay. These authors considered bispheres with a power law size distribution with  $v_{\text{eff}} = 0.2$  and  $r_{\text{eff}} = 1 \mu\text{m}$ . The computations were carried out at 628.3 nm with the refractive index fixed at  $1.5 + 0.005i$ . Although our measured results for fly ash particles at 442 nm do not clearly show this sudden decrease, Figure 3 seems to indicate that the decrease could start at higher angles for which we do not have measured results.

The measured  $F_{22}(\theta)/F_{11}(\theta)$  for fly ash decreases from almost 1 at angles close to the forward direction to a minimum at side-scattering angles and increases again at backscattering angles to high values (see Tables 6 and 7). As shown in Figure 3,  $F_{22}(\theta)/F_{11}(\theta)$  at backward directions and at both wavelengths (442 and 663 nm) lies outside the domain occupied by the aerosol measurements of *Volten et al.* [2001]. A very similar shape of  $F_{22}(\theta)/F_{11}(\theta)$  with a sudden increase around  $130^\circ$  was again also found by *Mishchenko et al.* [1995] for the polydisperse randomly oriented bispheres mentioned above. Similar behavior was also obtained from calculations by *Mackowski and Mishchenko* [1996] for monodisperse aggregates of  $N$  spheres with a size parameter of the single sphere of 5 and  $N$  ranging from 2 to 5. The refractive index for these calculations was fixed to  $1.5 + 0.005i$ . Although the shape of the measured  $F_{22}(\theta)/F_{11}(\theta)$  curve for fly ash particles is quite similar to that of the results for bispheres, the minimum of this ratio for our fly ash particles is much lower (0.5) than for the bispheres considered ( $\sim 0.7$ ). However, according to *Mackowski and Mishchenko* [1996], the minimum value of  $F_{22}(\theta)/F_{11}(\theta)$

**Table 4.** Maximum and Minimum Values of  $-F_{12}(\theta)/F_{11}(\theta)$  and  $F_{34}(\theta)/F_{11}(\theta)$  at 442 nm and Angles at Which These Values Are Reached<sup>a</sup>

Sample	$-F_{12}(\theta)/F_{11}(\theta); \theta$		$F_{34}(\theta)/F_{11}(\theta); \theta$	
	maximum	minimum	maximum	minimum
Fly ash	0.06 ; $100^\circ$	-0.02 ; $170^\circ$	0.20 ; $165^\circ$	-0.04 ; $10^\circ$
Green clay	0.18 ; $95^\circ$	-0.02 ; $170^\circ$	0.09 ; $75^\circ$	-0.01 ; $5^\circ$
Red clay	0.16 ; $95^\circ$	-0.01 ; $172^\circ$	0.09 ; $80^\circ$	-0.01 ; $10^\circ$
Av.Sc.M.	0.12 ; $105^\circ$	-0.02 ; $172^\circ$	0.11 ; $90^\circ$	-0.02 ; $15^\circ$

<sup>a</sup>The results are compared with those obtained for the average aerosol scattering matrix (Av.Sc.M.).

**Table 5.** Same as Table 4, but at 633 nm

Sample	$-F_{12}(\theta)/F_{11}(\theta); \theta$		$F_{34}(\theta)/F_{11}(\theta); \theta$	
	maximum	minimum	maximum	minimum
Fly ash	0.01 ; 25°	-0.12 ; 160°	0.23 ; 155°	-0.06 ; 15°
Green clay	0.22 ; 95°	-0.02 ; 171°	0.10 ; 70°	-0.01 ; 5°
Red clay	0.17 ; 95°	-0.02 ; 172°	0.10 ; 75°	-0.01 ; 5°
Av.Sc.M.	0.12 ; 105°	-0.02 ; 172°	0.11 ; 90°	-0.02 ; 15°

depends significantly on the number of single spheres  $N$  in the aggregate; the higher  $N$ , the lower the minimum of  $F_{22}(\theta)/F_{11}(\theta)$ . Thus the difference in the minimum values of  $F_{22}(\theta)/F_{11}(\theta)$  for our measured results and the calculated results by *Mishchenko et al.* [1995] could be due to the number of single-constituent spheres in the calculations being too small for an adequate model of our fly ash particles.

**4.3. Discussion of the Scattering Matrices of Clay Particles.**

We present in Figures 4 and 5 results of the experimentally determined scattering matrices of green clay and red clay particles at 442 and 633 nm, respectively, together with the average scattering matrix. The measured angular distributions of scattering matrix elements for green clay and red clay generally agree with the curves presented by the average of irregular shaped mineral particles. Note that the red clay results are included in this average. Since green clay and red clay particles have practically identical shapes and size distributions (see section 2), any differences in their scattering behavior (see Figures 4 and 5) are most likely due to small differences in the refractive indices of the samples.

For both clays the scattering functions or phase functions  $F_{11}(\theta)$  are smooth functions of the scattering angle showing a strong forward peak; they are featureless and flat at side-scattering angles and have almost no structure at backscattering angles. This scattering behavior, as mentioned before, seems to be a general property of ensembles of mineral irregular particles [*Jaggard et al.*, 1981; *West et al.*, 1997; *Mishchenko et al.*, 2000b; *Volten et al.*, 2001]. The values of the steepness of the  $F_{11}(\theta)$  curves are also quite similar for both clays (see Table 3).

The measured  $-F_{12}(\theta)/F_{11}(\theta)$  curves, which in our case equal the degree of linear polarization for unpolarized incident light, have similar bell shapes. They show a maximum at side-scattering angles with a negative branch at positions close to the backward direction. For small particles with sizes smaller than or approximately equal to the wavelength and a refractive index that remains the same, the maximum of  $-F_{12}(\theta)/F_{11}(\theta)$  is expected to increase if the size parameter of the particles decreases [*Mishchenko et al.* 2000c]. The results of the measurements for green clay particles illustrate this effect. When going from 442 to 633 nm, which causes the size parameter to become smaller, the maximum value of  $-F_{12}(\theta)/F_{11}(\theta)$  increases from 0.18 at 442 nm to 0.22 at 633 nm (see Tables 4 and 5). For the red clay particles this behavior is less pronounced. The maximum values of  $-F_{12}(\theta)/F_{11}(\theta)$  obtained for the red clay particles are quite similar at both wavelengths, that is, 0.16 at 442 nm and 0.17 at 633 nm (see Tables 4 and 5). This may be explained by differences in the imaginary part of the refractive indices of both samples. The red color of the red clay particles suggests that the imaginary part of the refractive index of the red clay particles is lower at 633 nm than at 442 nm. Since small particles tend to show less polarization if the absorption decreases [see e.g. *Mishchenko and Travis*, 1994], it seems that for this sample the effect of a smaller size parameter is nearly compensated by less absorption occurring in the particles at 633 nm.

The ratios  $F_{34}(\theta)/F_{11}(\theta)$  of the green and red clay particles differ very little at both wavelengths. Therefore we may conclude that this ratio is probably not very sensitive to small differences in refractive index.

Small differences depending on the wavelength are found for the  $F_{33}(\theta)/F_{11}(\theta)$  and  $F_{44}(\theta)/F_{11}(\theta)$  ratios. The  $F_{33}(\theta)/F_{11}(\theta)$  curves of the two clays present rela-

**Table 6.** Maximum and Minimum Values of  $F_{22}(\theta)/F_{11}(\theta)$  and Angles at Which These Values Are Reached<sup>a</sup>

Sample	$F_{22}(\theta)/F_{11}(\theta); \theta$		$F_{22}/F_{11}(173^\circ)$
	maximum	minimum	
Fly ash	0.90 ; 10°	0.49 ; 120°	0.80
Green Clay	0.91 ; 5°	0.33 ; 120°	0.43
Red clay	0.96 ; 5°	0.41 ; 110°	0.54
Av.Sc.M.	0.96 ; 5°	0.31 ; 130°	0.42

<sup>a</sup>Values of  $F_{22}(\theta)/F_{11}(\theta)$  at 173° These results have been obtained at 442 nm and are compared with those obtained for the average aerosol scattering matrix (Av.Sc.M.).

**Table 7.** Same as Table 6, but at 633 nm

Sample	$F_{22}(\theta)/F_{11}(\theta)$ ; $\theta$ , deg.		$F_{22}/F_{11}(173^\circ)$
	maximum	minimum	
Fly ash	0.90 ; $5^\circ$	0.49 ; $135^\circ$	0.73
Green Clay	0.93 ; $5^\circ$	0.40 ; $125^\circ$	0.50
Red clay	0.96 ; $5^\circ$	0.38 ; $120^\circ$	0.48
Av.Sc.M.	0.96 ; $5^\circ$	0.31 ; $130^\circ$	0.42

tive to each other a different behavior at both 442 and 633 nm. The measurements for green clay particles at 633 nm are above the red clay curve up to about  $130^\circ$ , where the measurements for red clay particles become higher. In contrast, the results at 442 nm show the opposite behavior; the red clay curve is higher at small scattering angles up to about  $50^\circ$  where green clay measurements become higher. This different wavelength dependence is probably also due to the differences in the complex refractive index of the particles.

## 5. Conclusions

In this work we present measurements of the scattering matrix as a function of the scattering angle of three samples of randomly oriented mineral particles as examples of two of the classes in which small particles can be divided: aggregates (fly ash) and compact particles (green clay and red clay). The measurements have been carried out at two wavelengths, 442 and 633 nm.

First, we have studied the influence of the shape of the particles on the scattering patterns (section 4.2). For this purpose the measured results for the fly ash particles have been compared to the average scattering matrix obtained by *Volten et al.* [2001] for a broad selection of compact particles (including red clay) and the same two wavelengths. Although detailed differences are present in the measured scattering matrices, the construction of this average was justified by the high similarity in scattering behavior of the seven compact samples on which the average is based. Our experimental results for fly ash particles show appreciable differences from this average aerosol scattering matrix, that is, a strong increase of  $F_{11}(\theta)$  at backward directions, small values of  $-F_{12}(\theta)/F_{11}(\theta)$ , a maximum of  $F_{34}(\theta)/F_{11}(\theta)$  at large scattering angles, a strong increase of  $F_{22}(\theta)/F_{11}(\theta)$  near backscattering angles and sudden decreases of  $F_{33}(\theta)/F_{11}(\theta)$  and  $F_{44}(\theta)/F_{11}(\theta)$  near backscattering angles. Moreover, appreciable parts of the curves representing the angular dependence of the scattering matrix elements for the fly ash particles lie outside the domains occupied by the aerosol measurements of *Volten et al.* [2001]. These differences can only be attributed to the marked difference in shape of the fly ash particles, since the other properties (size distributions and refractive indices) fall within the ranges that are valid for the aerosol samples considered by *Volten et al.* [2001]. In addition, we found that the scattering matrix elements for fly ash particles (except  $F_{22}(\theta)/F_{11}(\theta)$ ) resemble results of Mie calculations for

polydisperse spheres with similar size distributions as the constituent particles.

Therefore these differences indicate that scattering properties of polydisperse samples of aggregates of nearly spherical mineral particles tend to differ considerably from those of compact mineral particles. In fact, we compared scattering matrices of individual compact mineral aerosol samples, as presented by *Volten et al.*, [2001], with the scattering matrices of fly ash and found similar differences for all samples of compact particles, which is consistent with the fact that the scattering matrix elements of fly ash lie outside the domain covered by the compact mineral aerosol particles. More measurements with different types of aggregates are needed to establish general trends for such particles. In that manner, an average scattering matrix might be obtained in the same way that *Volten et al.* [2001] did for compact mineral particles. This average could then be used as a diagnostic tool for the detection of aggregates in, for example, astronomical observations.

Second, we have studied the influence of small differences in composition on the scattering behavior (section 4.3). The compositions of the green and red clay particles do not differ very much and their size distributions and shapes are almost identical. Therefore the differences in the measured scattering matrices for these two samples of clays, namely, slightly different steepnesses of  $F_{11}(\theta)$ , different maximum of  $-F_{12}(\theta)/F_{11}(\theta)$ , and small differences in  $F_{33}(\theta)/F_{11}(\theta)$  and  $F_{44}(\theta)/F_{11}(\theta)$ , are probably due to the small differences in their composition. The most striking result is related to the  $-F_{12}(\theta)/F_{11}(\theta)$  ratio. Reasoning about the polarization properties of small particles is often based on the general rule that the polarization tends to increase if the size parameter becomes smaller (see the  $-F_{12}(\theta)/F_{11}(\theta)$  results for green clay particles at both wavelengths). However, such a rule assumes that the rest of the parameters stays the same. Here we give an example (red clay) in which the polarization hardly increases if the effective size parameter becomes smaller, which seems to violate the general rule. This apparent violation of the rule can be explained if we account for changes in the refractive index of the particles with wavelength. This shows that the general rule has limited validity for strongly colored particles.

**Acknowledgments.** We are indebted to R. D. Schuiling from the University of Utrecht for providing the fly ash sample. The clay samples were provided by Argiletz, S.A. in France. We are grateful to several people of the Free University, particularly to J. Bouma for technical support, M.

Konert for measuring the size distributions of the samples, and S. Kars for providing SEM photographs of our samples. Information on the clay samples was kindly provided by K. Nadia of Argiletz. This work was performed under ESA external fellowship at the Department of Physics and Astronomy, Free University, Amsterdam.

## References

- Bottiger, J. R., E. S. Fry, and R. C. Thompson, Phase matrix measurements for electromagnetic scattering by sphere aggregates, in *Light Scattering by Irregularly Shaped Particles*, edited by D.W. Schuerman, pp. 283-290, (Plenum, New York), 1980.
- Charlson, R. J., S. E. Schwartz, J. M. Hales, R. D. Cess, J. A. Coakley Jr., J. E. Hansen, and D. J. Hofmann, Climate forcing by anthropogenic aerosols, *Science*, *255*, 423-430, 1992.
- Colangeli, L., V. Mennella, C. Di Marino, A. Rotundi, and E. Bussoletti, Simulation of the cometary 10 $\mu$ m band by means of laboratory results on silicatic grains, *Astron. Astrophys.*, *293*, 927-934, 1995.
- d'Almeida, G. A., P. Koepke, and E. P. Shettle, Atmospheric aerosols, in *Global Climatology and Radiative Characteristics*, A. Deepak, Hampton, Va., 1991.
- Egan, W. G., and T. W. Hilgeman, *Optical Properties of Inhomogeneous Materials: Applications to Geology, Astronomy, Chemistry, and Engineering*, Academic, San Diego, Calif., 1979.
- Gerber, H. E., and Hindman, (Eds.), Light absorption by aerosol particles, in *Technical Proceedings of the First International Workshop on Light Absorption by Aerosol Particles, Fort Collins, Col., 1980*, Spectrum, Hampton, Va., 1982.
- Greenberg, J. M., and B. Å. S. Gustafson, A comet fragment model for zodiacal light particles, *Astron. Astrophys.*, *93*, 35-42, 1981.
- Gustafson B. Å., Microwave analog to light-scattering measurements, in *Light Scattering by Nonspherical Particles*, edited by M. I. Mishchenko, J. W. Hovenier, and L. D. Travis, pp. 367-389, Academic, San Diego, Calif., 2000.
- Gustafson, B. Å. S., and L. Kolokolova, A systematic study of light scattering by aggregate particles using the microwave analog technique: Angular and wavelength dependence of intensity and polarization, *J. Geophys. Res.*, *104*, 31,711-31,720, 1999.
- Hansen, J. E., and L. D. Travis, Light scattering in planetary atmospheres, *Space Sci. Rev.*, *16*, 527-610, 1974.
- Haubebourg, V., M. Cabane, and A. C. Levasseur-Regourd, Theoretical polarimetric responses of fractal aggregates, in relation with experimental studies of dust in the solar system, *Phys. Chem. Earth*, *24*, 603-608, 1999.
- Hodkinson, J., Light scattering and extinction by irregular particles larger than the wavelength, in *Electromagnetic Scattering*, edited by M. Kerker, pp. 87-100, N. J., Macmillan, Old Tappan, New York, 1963.
- Holland, A. C., and G. Gagne, The scattering of light by polydisperse systems of irregular particles, *Appl. Opt.*, *28*, 2389-2400, 1970.
- Hovenier, J. W., Measuring scattering matrices of small particles at optical wavelengths, in *Light Scattering by Nonspherical Particles*, edited by M. I. Mishchenko, J. W. Hovenier, and L. D. Travis, pp. 355-365, Academic, San Diego, Calif., 2000.
- Hovenier, J. W., and C. V. M. van der Mee, Fundamental relationships relevant to the transfer of polarized light in a scattering atmosphere, *Astron. Astrophys.*, *128*, 1-16, 1983.
- Hovenier, J. W., and C. V. M. van der Mee, Testing scattering matrices, a compendium of recipes, *J. Quant. Spectrosc. Radiat. Transfer*, *55*, 649-661, 1996.
- Jäger, C., H. Mutschke, B. Begemann, J. Dorschner, and T. Henning, Steps toward interstellar silicate mineralogy, I., Laboratory results of a silicate glass of mean cosmic composition, *Astron. Astrophys.*, *292*, 641-655, 1994.
- Jaggard, D. L., C. Hill, R. W. Shorthill, D. Stuart, M. Glantz, F. Rosswog, B. Taggard, and S. Hammond, Light scattering from particles of regular and irregular shape, *Atmos. Environ.*, *15*, 2511-2519, 1981.
- Kerr, P. F., *Optical Mineralogy*, McGraw-Hill, New York, 1959.
- Klein, C., and C. S. Hurlbut Jr., *Manual of Mineralogy*, John Wiley, New York, 1993.
- Konert, M., and J. Vandenberghe, Comparison of laser grain size analysis with pipette and sieve analysis: A solution for the underestimation of the clay fraction, *Sedimentology*, *44*, 532-535, 1997.
- Kuik, F., P. Stammes, and J. W. Hovenier, Experimental determination of scattering matrices of water droplets and quartz particles, *Appl. Opt.*, *30*, 4872-4881, 1991.
- Lumme, K., Scattering properties of interplanetary dust particles, in *Light Scattering by Nonspherical Particles*, edited by M. I. Mishchenko, J. W. Hovenier, and L. D. Travis, pp. 555-582, Academic, San Diego, Calif., 2000.
- Lumme, K., J. Rahola, and J. W. Hovenier, Light scattering by dense clusters of spheres, *Icarus*, *126*, 455-469, 1997.
- Mackowski, D. W., Electrostatic analysis of radiative absorption by bisphere clusters in the Rayleigh limit: Application to soot particles, *Appl. Opt.*, *34*, 3535-3545, 1995.
- Mackowski, D. W., and M. I. Mishchenko, Calculation of the T matrix and the scattering matrix for ensembles of spheres, *J. Opt. Soc. Am. A Opt. Image Sci.*, (11) 2266-2278, 1996.
- Mishchenko, M. I., and D. W. Mackowski, Electromagnetic scattering by randomly oriented bispheres: Comparison with experiment and benchmark results, *J. Quant. Spectrosc. Radiat. Transfer*, *55*, 683-694, 1996.
- Mishchenko, M. I., and L. D. Travis, Light scattering by polydisperse, rotationally symmetric nonspherical particles: Linear polarization, *J. Quant. Spectrosc. Radiat. Transfer*, *51*, 759-778, 1994.
- Mishchenko, M. I., D. W. Mackowski and L. D. Travis, Scattering of light by bispheres with touching and separated components, *Appl. Opt.*, *34*, 4589-4599, 1995.
- Mishchenko, M. I., J. W. Hovenier, and L. D. Travis, (Eds.), *Light Scattering by Nonspherical Particles*, Academic, San Diego, Calif., 2000a.
- Mishchenko, M. I., W. J. Wiscombe, J. W. Hovenier, and L. D. Travis, Overview of scattering by nonspherical particles, in *Light Scattering by Nonspherical Particles*, edited by M. I. Mishchenko, J. W. Hovenier, and L. D. Travis, pp. 30-59, Academic, San Diego, Calif., 2000b.
- Mishchenko, M. I., L. D. Travis, and A. Macke (Eds.), T-matrix method and its applications, in *Light Scattering by Nonspherical Particles*, edited by M. I. Mishchenko, J. W. Hovenier, and L. D. Travis, pp. 147-170, Academic, San Diego, Calif., 2000c.
- Molster, et al., Low-temperature crystallization of silicate dust in circumstellar disks, *Nature*, *40*, 563-565, 1999.
- Moroz, V. I., Y. M. Gektin, M. K. Naraeva, A. S. Selivanov, and D. V. Titov, Aerosol vertical profile on Mars from the measurements of thermal radiation on the limb, *Planet. Space Sci.*, *42*, 831-846, 1994.
- Muñoz, O., H. Volten, J. de Haan, W. Vassen, and J. W. Hovenier, Scattering matrices of olivine and Allende meteorite particles, *Astron. Astrophys.*, *360*, 777-788, 2000.
- Okada, K., A. Kobayashi, Y. Iwasaka, H. Naruse, T. Tanaka, and O. Nemoto, Features of individual Asian dust-storm

- particles collected at Nagoya, Japan, *J. Meteorol. Soc. Jpn.*, *65*, 515-521, 1987.
- Perry, R. J., A. J. Hunt, and D. R. Huffman, Experimental determinations of Mueller scattering matrices for nonspherical particles, *Appl. Opt.*, *17*, 2700-2710, 1978.
- Prospero, J. M., R. A. Glaccum, and R. T. Nees, Atmospheric transport of soil dust from Africa to South America, *Nature*, *289*, 570-572, 1981.
- Rietmeijer, F. J. M., A model for tropical-extratropical transport of volcanic ash in the lower stratosphere, *Geophys. Res. Lett.*, *20*, 951-954, 1993.
- Tröger, W. E., H. U. Bambauer, F. Taborsky, and H. D. Trochim, *Optische Bestimmung der gesteinsbildenden Minerale Teil I: Bestimmungstabellen*, Schweizerbart, Stuttgart, Germany, 1971.
- Van de Hulst, H. C., *Light Scattering by Small Particles*, John Wiley, New York, 1957.
- Volten, H., O. Muñoz, E. Rol, J. F. de Haan, W. Vassen, J. W. Hovenier, K. Muinonen, and T. Nousianen, Scattering matrices of mineral aerosol particles at 441.6 nm and 632.8 nm, *J. Geophys. Res.* *106*, p. 17,375, 2001.
- Warren, J. L., M. E. Zolensky, K. Thomas, A. L. Dodson, L. A. Watts, and S. Wentworth, *Cosmic Dust Cat. 15*, NASA, Houston, Tex., 1997.
- Weiss-Wrana, K., Optical properties of interplanetary dust: Comparison with light scattering by larger meteoritic and terrestrial grains, *Astron. Astrophys.*, *126*, 240-250, 1983.
- West, R. A., Optical properties of aggregate particles whose outer diameter is comparable to the wavelength, *Appl. Opt.*, *30*, 5316-5324, 1991.
- West, R. A., and P. H. Smith, Evidence for aggregate particles in the atmospheres of Titan and Jupiter, *Icarus*, *90*, 330-333, 1991.
- West, R. A., L. R. Doose, A. M. Eibl, M. G. Tomasko, and M. I. Mishchenko, Laboratory measurements of mineral dust scattering phase function and linear polarization, *J. Geophys. Res.*, *102*, 16,871-16,881, 1997.
- Wurm, G., and J. Blum, Experiments on preplanetary dust aggregation, *Icarus*, *132*, 125-136, 1998.
- Xing, Z., and M. Hanner, Light scattering by aggregate particles, *Astron. Astrophys.*, *324*, 805-820, 1997.
- Xu, Y. L., and B. Å. S. Gustafson, Comparison between multisphere light-scattering calculations: (I) Rigorous solution and (II) DDA, *Astrophys. J.*, *513*, 896-911, 1999.
- Yanamandra-Fisher, P. A., and M. S. Hanner, Optical properties of nonspherical particles of size comparable to the wavelength of light: Application to comet dust, *Icarus*, *138*, 107-128, 1999.

---

J. F. de Haan, J. W. Hovenier, W. Vassen, and H. Volten  
Department of Physics and Astronomy, Free University, De  
Boelelaan 1081, NL-1081 HV Amsterdam, Netherlands.

O. Muñoz, Instituto de Astrofísica de Andalucía, CSIC,  
P.O. Box 3004, Granada, 18080, Spain. (olga@iaa.es)

(Received November 14, 2000; revised April 2, 2001;  
accepted June 11, 2001.)